Angular shape of the oceanic particulate volume scattering function in the backward direction

James M. Sullivan* and Michael S. Twardowski

WET Labs, Inc., Department of Research, 70 Dean Knauss Drive, Narragansett, Rhode Island 02882, USA

*Corresponding author: jims@wetlabs.com

Received 5 August 2009; revised 12 October 2009; accepted 1 November 2009; posted 9 November 2009 (Doc. ID 115338); published 4 December 2009

Analysis of several million particulate volume scattering functions (VSFs) from different field sites around the world's oceans and coastlines revealed that the shape of the VSF in the backward direction was remarkably consistent (5% or less variability at angles between 90° and 170°). In agreement with theoretical models and past field measurements, the variability of the VSF shape (the VSF normalized to the backscattering coefficient) was found to be lowest between 110° and 120°. This study concludes that under most oceanic conditions, estimates of the particulate backscattering coefficient, using single angle scattering measurements near 110° to 120° and suitable conversion factors, are justified and should have a maximum uncertainty of less than a few percent once instrument noise is accounted for. © 2009 Optical Society of America

OCIS codes: 010.4450, 000.2170, 120.5820, 290.1350, 350.4990.

1. Introduction

The volume scattering function (VSF), $\beta(\theta)$ (units of $m^{-1}\,sr^{-1}$), describes the angular (θ) dependence of scattered light from an incident unpolarized beam. Assuming azimuthal symmetry, integrating the VSF from 0 to π radians (or 0° to 180°) yields the scattering coefficient, b (units of m^{-1}), according to $2\pi \int \sin(\theta)\beta(\theta)d\theta$. Integrating the VSF in the backward direction (i.e., over $\pi/2$ to π radians, or 90° to 180°) yields the backscattering coefficient, b_b (units of m^{-1}), which is of particular importance to remote sensing, as remote sensing reflectance is approximately proportional to: $b_b/(a+b_b)$ [1]. In fact, the shape of the upwelling radiance distribution, described with respect to the downwelling incident light field by the bidirectional reflectance distribution function (BRDF), has been shown to be largely governed by the shape of the VSF [2–5]. Moreover, the inherent optical properties (IOPs), i.e., the VSF and absorption properties of a water mass, form the link between its biogeochemical constituents (phytoplankton, detrital material, and inorganic minerals) and the apparent optical properties (AOPs). Understanding this interrelationship is at the heart of successfully carrying out inversions of satellite-measured radiance to biogeochemical properties.

In practice, it is difficult to measure the full VSF due to (1) the complex design of instrumentation required to make a large number of discrete measurements over a broad angular range, especially at the near-forward (the first several degrees) and far-backward angles (the last several degrees), and (2) the large dynamic range in signal that must be resolved (typically greater than 4 orders of magnitude in a single VSF). Petzold [6] approached this problem by using two separate devices: the Low Angle Scattering Meter (LASM) that resolved the steeply peaked near-forward VSF at two angles (0.169° and 0.338°) and the General Angle Scattering Meter (GASM) that resolved the rest of the VSF in 10° increments with additional measurements at 15° and 25°. Higher resolution VSF data were generated from interpolation. Kullenberg [7] used a similar approach, measuring near-forward angles of the VSF (1°, 2.5°, and 3.5°) with a laser device and

0003-6935/09/356811-09$15.00/0

supplementing these data with discrete measurements over a broader angular range (10° to 165°) using a VSF device developed by Jerlov [8]. It should be noted that Kullenberg's laser was polarized and his near-forward VSF measurements should be treated accordingly. Nonetheless, these pioneering efforts produced valuable but very limited numbers of oceanic measurements. Currently, we are aware of two instruments capable of measuring the VSF *in situ* over a broad angular range. One is the Multispectral Volume Scattering Meter (MVSM or VSM) [9], with the current iteration measuring the VSF at eight wavelengths at angles between 0.6° and 177.9° at 0.3° intervals [10,11]. The other is the instrument used in this study: the Multi-Angle SCattering Optical Tool (MASCOT). The MASCOT was recently developed by WET Labs (Philomath, Oregon) and measures the VSF of monochromatic light (658 nm) between 10° and 170° at 10° intervals [12].

With instruments that measure the VSF with sufficient angular resolution in the backward direction (e.g., the MVSM or MASCOT), computing backscattering coefficients is a straightforward integration. Because of the current limited availability of multiangle VSF sensors, however, researchers needing to resolve backscattering coefficients typically make volume scattering measurements at a single or several angles and estimate the b_b using suitable conversion coefficients (termed χ factors) based on both modeled and/or measured VSF shape analysis in the backward direction [10,11,13–15]. Commercial instruments that employ these designs and methods are widely available and routinely deployed around the world's oceans (e.g., WET Labs' ECO sensors and HobiLabs' HydroScat sensors).

Assessing both the shape of the VSF in the backward direction and the reliability and potential errors associated with using single angle conversion factors for estimates of the b_b in variable oceanic environments is important for assessing errors in remote sensing validation, algorithm development, and for biogeochemical proxy applications. Although there appears to be growing consensus that measuring the VSF at an angle around 120° is optimal for estimating the backscattering coefficient [11,13,15], some results have suggested other optimal angles [10,14]. Moreover, there are two important concerns with these previous results that merit a detailed reanalysis: (1) the modeling in these studies was carried out with Mie theory, which assumes a homogeneous, spherical particle population that may not be representative of natural particle fields, especially in the backward direction of the VSF [16], and (2) the VSF measurements used in the analyses were typically made in a single oceanic region that may not be representative of the full variety of VSF shapes observed throughout the world's coastal and open oceans. In fact, Boss and Pegau [15] specifically concluded in their study that more measurements of VSFs from natural waters were needed to better quantify the variability and errors associated with using χ factors. This study examines the variability in the shape of the VSF in the backward direction using several million MASCOT VSF measurements, resolved between 10° and 170°, from a wide range of oceanic and coastal environments and includes an assessment of the robustness of the relationships between b_{bp} and single angle backscattering measurements.

2. Methods

In situ measurements were collected from ten different coastal and oceanic environments: the Penobscot River watershed outflow off coastal Maine in October of 2006 (abbreviated PR); off the coast of Oahu, Hawaii, during March of 2007 (abbreviated HI); the New Jersey bight during May and November of 2007 and July of 2008 (abbreviated NJ0507, NJ1107, and NJ0708, respectively); the San Diego, California, surf zone (Scripps Pier) and ~30 km off the coast during January of 2008 (abbreviated SDS and SDC, respectively); the Southern Ocean near South Georgia Island during March–April of 2008 (abbreviated SO); the Santa Barbara Channel off the coast of Santa Barbara, California, during September of 2008 (abbreviated SBC); and the Ligurian Sea off Liguria, Italy, during October of 2008 (abbreviated LS). Measurements consisted of both vertical profiles and stationary time series and were collected using a profiling package equipped with, among other instruments, a WET Labs AC-S or AC-9, a Seabird (Bellevue, Washington) SBE49 CTD, and the WET Labs MASCOT (Fig. 1). A WET Labs DH-4 was used to power sensors and pumps and archive and time stamp the data for all instruments. Data from the instruments were merged together using synchronized time. After merging, all data were averaged to 1 m depth bins.

The AC-S measures the absorption (a) and attenuation (c) of all in water constituents except water: a_{pg} and c_{pg}. To obtain the total absorption coefficients, a_t, the pure water absorption coefficients of Pope and Fry [17] are added to the a_{pg} measurements. The AC-S was calibrated before and after each cruise, according to the method of Twardowski *et al.* [18] with corrections for temperature and

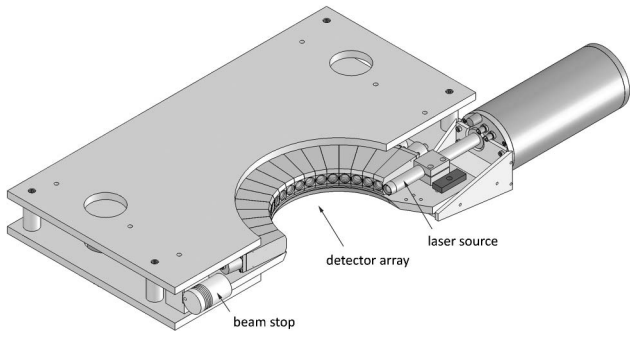

Fig. 1. Mechanical drawing of the MASCOT. The MASCOT has a semicircular array of 17 detector windows with a laser source and beam stop at each edge of the semicircle of detectors. The MASCOT has a length × width × height of ~86 cm × 38 cm × 15 cm.

salinity as described in Sullivan *et al.* [19]. Scattering errors in the AC-S absorption channels were corrected using the proportional correction algorithm of Zaneveld *et al.* [20]. AC-S measurements were used to correct for light losses along the MASCOT optical path during scattering measurements (see below).

The MASCOT measures the VSF in an open volume from 10° to 170° at 20 Hz. Its source beam is a 30 mW 658 nm laser diode expanded with a Galilean 2× beam expander to an approximately 3 × 8 mm elliptical shape. A wedge depolarizer is used to provide the unpolarized light needed for VSF determinations. Seventeen independent silicon diode detectors spaced in a semicircle 10 cm around the sample volume measure the volume scattering at 10° intervals. The total path length for all scattering measurements (distance from center of source window to center of sample volume to center of detector window) is 20 cm. Independent detectors allow resolution of the VSF without any moving parts and time-consuming scanning. Detector field-of-views (FOVs) range from 0.8° to 5° for the different detectors, with the narrowest FOVs associated with the detectors measuring scattering at the most forward angles. The MASCOT has a 20 Hz sampling rate for all channels and a worst case signal:noise of 300 : 1 for total scattering levels of approximately 0.1 m^{-1}. The MASCOT was designed to minimize the possibility of stray light contamination in measurements by (1) keeping the form factors of the detectors and associated structural elements as minimal as possible to avoid reflections, (2) using a collimated laser diode with a doubly reflected optical path, followed by a Gershun tube for the source optics, and (3) positioning a beam stop next to the 10° detector to extinguish the transmitted source beam to avoid any possible reflections.

Details of MASCOT use and calibration can be found in [12]. Briefly, to convert raw digital counts to volume scattering coefficients, $\beta(\theta)(m^{-1}\,sr^{-1})$, *in situ*, field determined dark counts (the meter's baseline reading in the absence of source light) (D) are subtracted from raw measurement counts (Φ) and the result multiplied by a scaling factor and attenuation correction:

$$\beta(\bar{\theta}_i) = [\Phi_i - D_i] f_i e^{L[b_p \epsilon + a_{pg} + a_w]}, \qquad (1)$$

where f is the scaling factor related to detector gain with units $m^{-1}\,sr^{-1}\,counts^{-1}$, L is the pathlength from source window to sample volume to detector window (nominally 20 cm), ϵ is the fraction of secondary scattering by particles that is not collected by the detector, b_p is the particulate scattering coefficient, a_{pg} is the absorption by particulate and dissolved material, and a_w is the absorption coefficient for pure water [17]. The i subscript represents the 17 individual detector channels, and the bar over θ signifies the centroid angle of the specific angular weighting for the ith scattering measurement.

The methods for MASCOT calibration are similar to that used for the WET Labs ECO sensor series [21], with the primary difference being that the longer pathlength of the MASCOT requires a more rigorous attenuation correction [12]. Scaling factors (f) are determined in the laboratory with solutions of microspherical beads (0.2 μm polystyrene beads, Thermo Scientific product 3200A) with traceable size distributions and a known refractive index [22]. The phase function, $[\beta_p(\theta/b_p)](sr^{-1})$, may be computed using Mie theory when the bead size distribution and refractive index are known. The angular weighting function for each scattering measurement, computed numerically, also must be included in this calculation (see Twardowski *et al.* [21]). Since b_p can be measured directly during laboratory calibration using concurrent WET Labs AC-S measurements (polystyrene absorption is negligible in comparison to bead scattering, so that the AC-S attenuation measurement can represent b_p with accuracy better than 1%), $\beta_p(\theta)$ may then be obtained for any concentration of beads as long as the b_p component of the theoretical phase function is obtained using an effective acceptance angle matching the AC-S or AC-9 attenuation measurement (0.93°). The factor ϵ is determined in the laboratory in solutions of a particle standard comprised of mineral particles encompassing a broad distribution over the size range important for scattering in hydrosols (Arizona Test Dust, ISO Ultrafine ATD 12103-1, Powder Technologies, Inc.). These solutions result in a scattering phase function very similar to that found in marine environments (e.g., Agrawal *et al.* [23]). Bead calibrations conducted over 1 y apart agreed at all angles within 5.8% in the worst case (median 2.7%). Calibrations were additionally validated with measurements in solutions of microspherical beads of other sizes than the calibration bead.

While MASCOT dark counts were determined in the laboratory, *in situ* field determinations were also made to ensure the highest accuracy possible in the final data, as *in situ* field dark count values might reflect specific instrumental configuration and environmental conditions during deployments [21]. *In situ* dark counts for the MASCOT were determined by covering the single laser source with black electrical tape and leaving all detectors exposed. Vertical profiles of dark counts were routinely conducted during each cruise (minimum of a few times per day and usually consecutively before or after each data profile) and the resulting *in situ* dark count values were applied individually for each cast during postprocessing, as described above.

Particulate backscattering coefficients (b_{bp}) from the MASCOT were determined by first removing the contribution to β_t by sea water using the Zhang *et al.* [24] formulation, then multiplying the resulting $\beta_p(\theta)$ values by $2\pi \sin(\theta)$, followed by a 1° interpolation using a Piecewise Cubic Hermite Interpolating Polynomial (MATLAB PCHIP function) of the $2\pi\beta_p(\theta)\sin(\theta)$ values between 90° and 170°,

including a value of zero at 180° as per the $\sin(\theta)$ term. A subsequent trapezoidal integration (MATLAB TRAPZ function) of the interpolated values yielded b_{bp}.

3. Results

In total, over three million MASCOT VSF measurements were collected during the ten field deployments and averaged into ~7000 1 m depth bins. The field sites represented a great diversity of coastal and oceanic water types from around the world's oceans (e.g., Pacific, Atlantic, Mediterranean, and Southern) and included surf-zone waters subject to resuspended sediments and intense bubble injection by waves (SDS), coastal waters with high chlorophyll (NJ0507, NJ1107) or riverine influence (PR), as well as clear oligotrophic waters (HI, LS, SO). Collectively, the β_p measurements in the backward direction spanned over 2 orders of magnitude [Fig. 2(a)]. For reference, the average b_{bp} values (and total range) from representative field sites were $\sim 0.0008\,\mathrm{m}^{-1}$ (range = 0.0004 to 0.001) for HI, $0.0015\,\mathrm{m}^{-1}$ (range = 0.0005 to 0.003) for SO, $\sim 0.0025\,\mathrm{m}^{-1}$ (range = 0.0004 to 0.03) for LS and SBC, $\sim 0.02\,\mathrm{m}^{-1}$ (range = 0.005 to 0.07) for NJ0507 and NJ1107, and $0.025\,\mathrm{m}^{-1}$ (range = 0.006 to 0.07) for PR.

In order to examine VSF shape variability in the backward direction (90° to 170°), the $\beta_p(\theta)$ measurements were normalized to b_{bp} to yield particulate phase functions in the backward direction ($\tilde{\beta}_{bp}$):

$$\tilde{\beta}_{bp} = \beta_p(\theta)/b_{bp}. \tag{2}$$

The combined $\tilde{\beta}_{bp}$ data from all field sites [Fig. 2(b)] and the average $\tilde{\beta}_{bp}$ from each individual field site [Fig. 2(c)] were similar, with a relatively flat shape at angles greater than 120°. The values of the average and standard deviation (σ) of $\tilde{\beta}_{bp}$ calculated from the combined 1 m binned field data are given in Table 1. A fourth-order polynomial fit of these data produced a line that was within <0.5% of the average $\tilde{\beta}_{bp}$ values (Table 2). The consistency in the $\tilde{\beta}_{bp}$ shape was remarkable given the great diversity of water types these measurements represent and the shapes of previously published VSFs [6]. For example, consider the average $\tilde{\beta}_{bp}$ from the combined field data (averaged after normalization) compared with the VSF shapes of the three distinct water types of Petzold [6]: turbid (San Diego harbor), coastal and clear (oligotrophic) [Fig. 3(a)]. For this comparison, the Petzold [6] VSF data were similarly averaged after normalization with the contribution of the backscattering by water removed (i.e., $\beta_p(\theta)/b_{bp}$). The turbid water type of Petzold [6] is somewhat comparable to the average of this study, although we measure a flatter shape at angles greater than 130°. The coastal and clear shapes of Petzold [6] are not similar and exhibit large increases at angles greater than 140°. It should be noted that the range in b_{bp} values measured in Petzold's study [6] was very similar to this

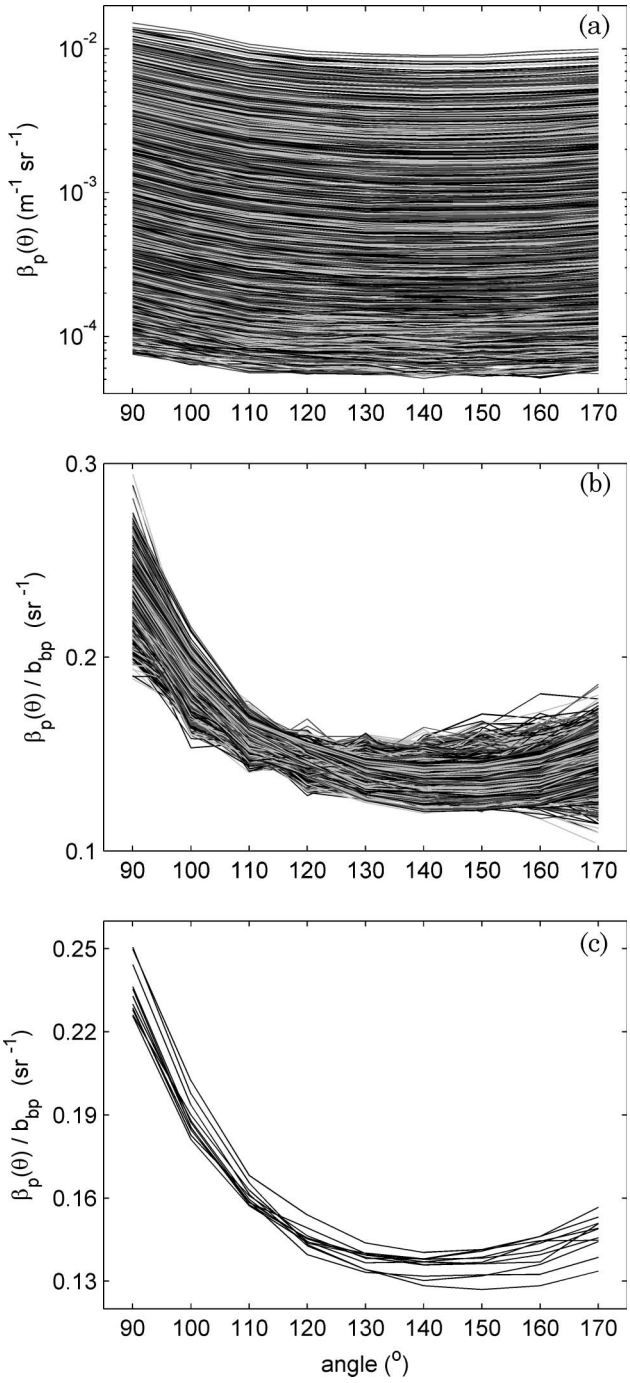

Fig. 2. (a) VSF in the backward angles from all field sites. (b) Phase functions in the backward direction ($\tilde{\beta}_{bp}$) from all field sites. (c) Average $\tilde{\beta}_{bp}$ from each of the ten field sites.

study, where Petzold's clear, oligotrophic water had a b_{bp} of $\sim 0.001\,\mathrm{m}^{-1}$, and his turbid water had a b_{bp} of $\sim 0.028\,\mathrm{m}^{-1}$. Additionally, our VSF database includes sites off San Diego and the coast of California, not far from where the Petzold coastal and turbid VSFs were collected.

A similar comparison between the average $\tilde{\beta}_{bp}$ from this study and analytically modeled Fournier–Forand (FF) particulate phase functions ($\tilde{\beta}_{FF}$) [25,26] showed remarkable similarity [Fig. 3(b)]. The FF

Table 1. Average, Standard Deviation (σ), and Percent Variability (σ as %) of $\tilde{\beta}_{bp}$ Yielded from the Combined Data of All Field Sites

Angle (°)	90	100	110	120	130	140	150	160	170
Avg.	0.233	0.186	0.159	0.145	0.138	0.137	0.138	0.141	0.146
σ	0.012	0.007	0.004	0.004	0.005	0.006	0.007	0.007	0.008
%	5	4	2	3	4	4	5	5	5

Table 2. Coefficients for a Fourth-Order Polynomial Fit of the Average Data[a]

Coefficient	a1	a2	a3	a4	a5
	5.885E – 09	–3.526E – 06	8.007E – 02	–8.150E – 02	3.266

[a]The 95% confidence interval about the polynomial fit was ±0.0135.

function is an analytical two-parameter approximation with the inputs being the hyperbolic slope (differential Junge type) of the particle size distribution (μ) and the real bulk index of refraction of the particles (n_p). An array of μ and n_p values representing the range estimated at the different field sites were used as input into the FF model. The range of values of μ and n_p were estimated from the field data using the models of Boss *et al.* [27] and Twardowski *et al.* [28], respectively, and for μ were between 3 and 4 (at 0.1 increments), and for n_p were between 1.02 and 1.18 (at 0.02 increments). This input array range was also a good representation of the range found in most natural waters [28–30]. The average of $\tilde{\beta}_{FF}$ shapes calculated from the input array and the average $\tilde{\beta}_{bp}$ of this study were within 2% or less for angles between 90° and 140°. There was a slightly larger difference (but still less than 5%) at angles greater than 140°, where the $\tilde{\beta}_{bp}$ of this study was somewhat flatter (lower). The angular variability (σ) of $\tilde{\beta}_{FF}$ shapes calculated from the input array and the $\tilde{\beta}_{bp}$ angular variability measured from the combined field sites were also very similar, where both show a minimum between angles of 110° and 120° and maximums at 90° and 170° [Fig. 3(b)].

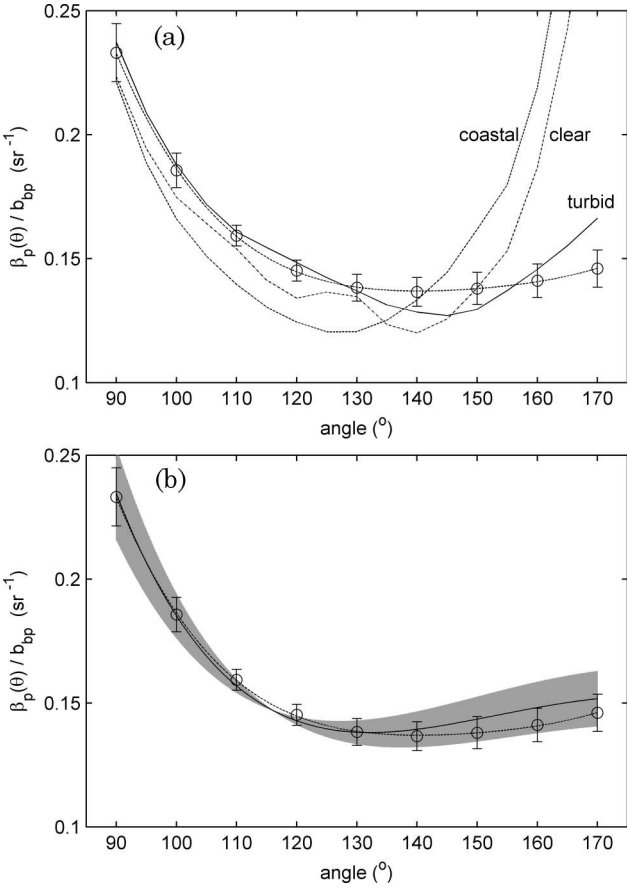

Fig. 3. (a) Average and standard deviation (σ) of $\tilde{\beta}_{bp}$ using MASCOT data from all field sites [open circles with error bars (σ) and dotted curve] compared to the $\tilde{\beta}_{bp}$ of Petzold's [6] three water types (turbid, coastal, and clear). (b) Average and σ of $\tilde{\beta}_{bp}$ using MASCOT data from all field sites [open circles with error bars (σ) and dotted curve] compared to the $\tilde{\beta}_{FF}$ analytical model values (shaded area). The solid curve through the center of the shaded area represents the average $\tilde{\beta}_{FF}$ with the width of the shading equal to the σ of the $\tilde{\beta}_{FF}$ values.

The combined MASCOT field data were used to calculate single angle empirical χ_p factors and their associated variability [Fig. 4(a)], where

$$\chi_p(\theta) = b_{bp}/2\pi\beta_p(\theta) = 1/2\pi\tilde{\beta}_{bp}(\theta). \quad (3)$$

The values of the average and σ of χ_p yielded from the combined field data are also given in Table 3. The χ_p factors of Boss and Pegau [15], Chami *et al.* [10] and Berthon *et al.* [11] are plotted for comparison [Fig. 4(a)]. For reference, the χ_p factors calculated over the entire angular range of the MASCOT are shown in Fig. 4(b). The values of Boss and Pegau [15] were within 5% or less of this study at all angles except 160° and 170°, where the differences increased to 12% and 43%, respectively. There was very close agreement (2% difference or less) between the angles of 120° and 150°. This was very similar to the χ_p factors determined using the average particulate phase functions of Berthon *et al.* [11], which were also within ~5% or less of this study at all angles except 160° and 170°. Also, similar to the Boss and Pegau [15] comparison, there was very close agreement (2% difference or less) for the Berthon *et al.* [11] χ_p factors between the angles of 110° and 150°. The χ_p factors (and overall $\tilde{\beta}_{bp}$ shape) of Chami *et al.* [10] were not similar to those of this study (~35% to 10% difference

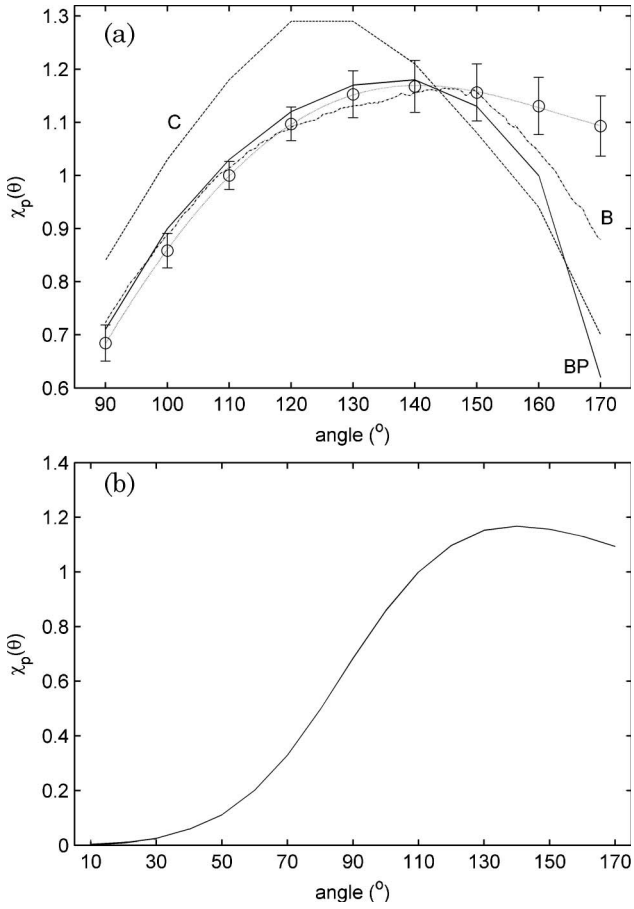

Fig. 4. (a) Average and standard deviations (σ) of χ_p factors using MASCOT data from all field sites [open circles with error bars (σ) and dotted curve]. The χ_p factors of Boss and Pegau [15] (solid curve marked "BP"), Chami *et al.* [10] (dashed curve marked "C") and Berthon *et al.* [11] (dashed–dotted curve marked "B") are plotted for comparison. (b) Average of χ_p factors using MASCOT data from all field sites over the full angular range of the instrument.

dependent on angle), with the exception of angles near 140° and 150° (~5% difference).

The minimum in the angular variability of $\tilde{\beta}_{bp}$ (and thus χ_p) in the backward direction was between 110° and 120° [Fig. 5(a)]. While the maximum variability at any angle was ~5% or less, a 1° cubic spline interpolation of these data indicated a minimum of ~2% at 113°. Similarly, χ_p factors calculated using the analytically derived $\tilde{\beta}_{FF}$ values indicated minimum variability (0.1%) at 116° [i.e., Fig. 3(b)]. These results indicate that estimates of the b_{bp} using χ_p factors from this study and accurate single angle measurements of β_p at angles near 110° to 120° should have a maximum uncertainty of only a few percent.

Remarkably, the actual uncertainty (or natural variability in $\tilde{\beta}_{bp}$) at these angles may be even less, as these measured uncertainties also include the random electronic noise of the MASCOT instrument itself. The numerous *in situ* dark count profiles taken with the MASCOT package allowed an examination of the magnitude of the MASCOT random electronic noise [Fig. 5(a) and 5(b)]. The magnitude of the MASCOT noise is a function of both the individual angular detectors and their gain settings. The MASCOT noise uncertainties tend to be largest in the backward angles, as overall signal is lower and higher electronic gain settings are required. For each field site, the electronic noise variability (i.e., the standard deviation of the *in situ* dark counts) was determined and converted to variability in terms of an absolute β value using the scaling factor. This value was scaled by the magnitude of the signal β values to determine the percent variability of the electronic noise uncertainty as a function of the signal magnitude at each location.

As expected, the natural measurement variability was greater than the instrument noise at all angles [Fig. 5(a)]. However, the measurement variability at 110° and 120° was very close to that of the instrument noise, with 120° exhibiting the lowest measurement variability relative to instrument noise. These results indicate that the actual uncertainty in $\tilde{\beta}_{bp}$ near 110° to 120° is apparently <1% and that the true minimum in the natural variability of $\tilde{\beta}_{bp}$ (and χ_p) is perhaps closer to 120° than 110°. Both of these hypotheses are supported by the analytically modeled VSF [25] results. It is interesting to note that the consistency in the VSF shape extends well into the forward angles with average uncertainties in χ_p factors of less than 10% for angles between ~50° to 90° [Fig. 5(b)].

4. Discussion

Over a very diverse array of water types representing different oceans, seasons and optical environments (e.g., oligotrophic, coastal, and even surf zone), with the accompanying diverse array and mixture of particle sizes and types, the shape of the $\tilde{\beta}_{bp}$ in the backward direction was found to be remarkably consistent (5% or less variability in standard error at any angle), with no distinct shape associated with any particular water type. Additionally, the average (and angular variability) of $\tilde{\beta}_{bp}$ empirically derived in this study was very similar to the average (and angular variability) of $\tilde{\beta}_{FF}$ analytically derived [25] using an input range representative of the range of values found throughout most of the world's oceans.

Table 3. Average and Standard Deviation (σ) of χ_p Yielded from the Combined Data of All Field Sites

Angle (°)	90	100	110	120	130	140	150	160	170
Avg.	0.684	0.858	1.000	1.097	1.153	1.167	1.156	1.131	1.093
σ	0.034	0.032	0.026	0.032	0.044	0.049	0.054	0.054	0.057

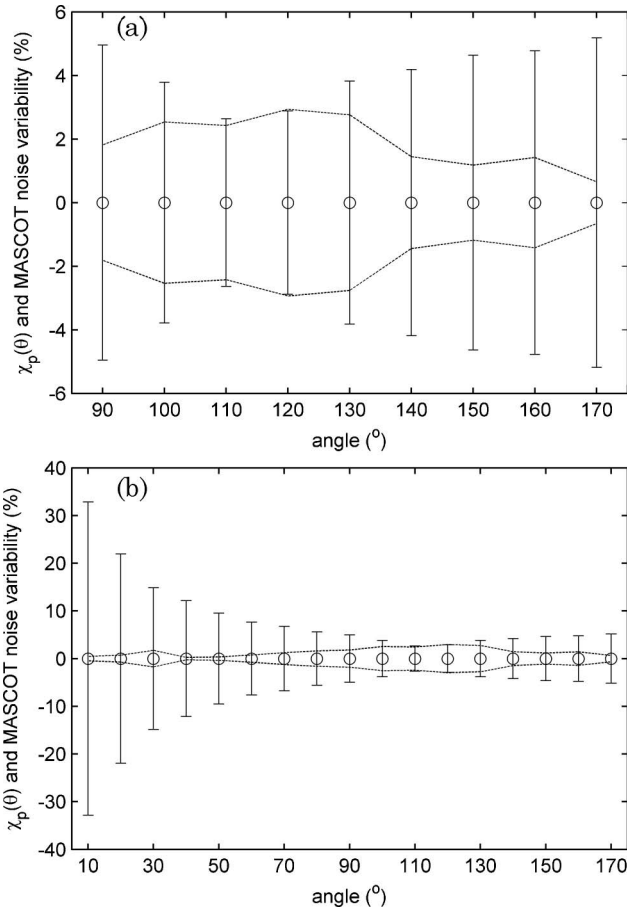

Fig. 5. (a) Percent variability (σ as %) in χ_p in the backward direction (open circles with error bars) compared to the random noise error of the MASCOT determined from dark count profiles (dotted curves). (b) Percent variability (σ as %) in χ_p over the full angular range of the MASCOT (open circles with error bars) compared to the random noise error of the MASCOT determined from dark count profiles (dotted curves).

These results lead to the surprising conclusion that, for the vast majority of oceanic conditions and water types, radiative transfer models for the ocean need only consider a single $\tilde{\beta}_{bp}$ in the backward direction where the single scattering approximation is valid. This has implications for the stability of the shape of the bidirectional reflectance distribution function (BRDF) important for remote sensing, since the shape of the radiance distribution around nadir, i.e., as viewed by satellites, is almost entirely dependent on the shape of the phase function in the backward direction [2,3,5]. A complicating factor is the *relative* contribution of molecular scattering by pure sea water to the total VSF. This requires that we also know the *magnitude* of b_{bp} to accurately predict the shape of the total phase function for remote sensing applications, at least for the relatively clear waters that comprise most of the global ocean. This leads to a paradox for coastal case II waters versus open ocean case I waters: although coastal waters are typically much more optically complex than clear open ocean waters, the fact that the particle contribution dominates the VSF in coastal waters (i.e., the water contribution is negligible in proportion), will result in a total phase function—and a shape for the upwelling radiance distribution relative to solar zenith—that should be more predictable, indeed, nominally constant in coastal waters.

Even though minimal variability in the shape of the phase function in the backward direction was observed, this does not suggest the shape of the phase function in general is relatively constant. The shape of the particulate VSF is primarily dependent on both the size distribution and refractive index of the particle assemblage and secondarily on particle shape and internal structure [30]. While the shape of the VSF in the forward direction, and the relative amount of near-forward scattering, is dominated by the size distribution of particles (and is the basis of laser diffraction particle sizing techniques), the composition (e.g., bulk refractive index) of the particles is most important in determining the relative amount of backscattering for natural oceanic particle populations [28–30]. The approximate observed range for the backscattering ratio (the ratio of particulate backscattering to total particulate scattering) in most oceanic environments covers about an order of magnitude (~0.3% to ~3%) [28,29,31,32]. A similar dynamic range was measured in this study.

The average $\tilde{\beta}_{bp}$ shape of this study decreased from 90° to 130°, remained flat between 130° and 160° (less than 3% difference between $\tilde{\beta}_{bp}$ values in this angular range), and slightly increased at 170° (to a value equivalent to 120°). The minimum in the $\tilde{\beta}_{bp}$ shape occurred at ~140°. There is some discrepancy between the consistency of the VSF shape found in this study and the VSF shapes from natural waters reported by others. For example, Petzold's [6] clear and coastal measurements and the MVSM field measurements of Boss and Pegau [15], Chami *et al.* [10] and Berthon *et al.* [11] tend to show increasing upwards curvature at angles greater than ~150° compared to the relatively flat $\tilde{\beta}_{bp}$ measured by the MASCOT and $\tilde{\beta}_{FF}$ modeled using the FF function [25,26]. Berthon *et al.* [11] noted that the sharp increases in MVSM measurements at larger angles in both field measurements, and in MVSM microsphere bead calibrations that did not agree with Mie theory, could be due to internal stray light reflections. It should be noted that although the MVSM is an *in situ* device, the sample is pumped through an inner flow cell, which, though allowing for benchtop applications, could also exacerbate reflection problems. With respect to the measurements of Petzold [6], we never observed the small peak in the clear water type VSF between 120° and 130° [Fig. 3(a)] or the appreciable increase Petzold observed toward the near backward for clear waters. While it is difficult to speculate on the cause of these discrepancies, these features seem unlikely.

Several researchers have analyzed the best fixed angle(s) to make backscattering measurements and the associated χ factors that should be used to

convert these measurements to backscattering coefficients. Oishi [13], using Mie scattering models and limited *in situ* VSF data (e.g., [6,7]) calculated χ factors at multiple angles in the backward direction and determined that scattering measured at an angle around 120° had the best correlation to b_b and the smallest prediction error. Maffione and Dana [14] argued in a reanalysis of Oishi's [13] results that using an angle ~140° was more appropriate, as this angle had the lowest maximum prediction error. However, after analysis of Mie modeled VSFs, Maffione and Dana [14] also concluded that the standard deviations of the average of numerous backward phase functions had a minimum over an angular range ~112° to 119°. Boss and Pegau [15] revisited the problem with extensive Mie scattering models and both historical and new *in situ* VSF data from an early version of the MVSM and found results consistent with those of Oishi [13]. They concluded that the tight relationship between b_b and scattering measurements near 120° was the result of two factors: first, for particle assemblages of different optical properties and size, the shape of the particulate VSF normalized to b_{bp} varies least ~120° (a result strongly supported by this study); and second, the ratio of the VSF to b_b is least sensitive near this angle to backscattering by water, b_{bw}. Thus, they concluded that the best angle to predict b_b would be where $\chi_p(\text{particles}) = \chi_w(\text{water})$ and they found this angle to be ~118°. In agreement with Boss and Pegau [15], Berthon *et al.* [11] found that in VSF measurements from the Adriatic Sea, $\chi_p = \chi_w$ at ~118°. Similar to these previous results, in this study, $\chi_p = \chi_w$ at ~119°, and the lowest angular variability was found to occur between 110° and 120°. However, in contrast to these results, Chami *et al.* [10] analyzed *in situ* VSF data collected by the MVSM during a three-week experiment along the coast of the Black Sea and reported that $\chi_p = \chi_w$ at ~110° and that $\tilde{\beta}_{bp}$ (and χ_p) varied significantly over the angular range of 100° to 130° and was least variable at ~140°. Chami *et al.* [10] concluded that using consistent χ_p factors at angles in the range of 110° to 130° may not be justified. However, to obtain the best agreement between theoretical models and their *in situ* VSF measurements, Chami *et al.* [10] needed to assume the presence of a population of monodispersed particles, which would likely indicate a rarely occurring oceanic condition. The results of our wide geographic study (and others) support the conclusion that under most oceanic conditions, the use of a consistent χ_p factor is justified.

5. Conclusions

Analysis of several million VSFs from many different field sites around the world's oceans and coastlines revealed that the variability of the VSF shape in the backward direction was very low (~5% or less variability at any angle between 90° and 170°). In agreement with both Mie [13–15] and FF models [23], the natural angular variability was lowest between 110° and 120° (2% or less). Thus, estimates of the b_{bp} using χ_p factors from this study and accurate single angle measurements of β_p at angles near 110° to 120° are justified and should have a maximum uncertainty of only a few percent.

Scott Freeman and Matt Slivkoff are thanked for providing assistance in data collection and processing. Jean-François Berthon is thanked for providing average phase function data from his 2007 publication [11]. Support for MASCOT sensor development and field work was provided by the Office of Naval Research Environmental Optics, contract N0001406C0027. Additional support for field efforts was provided by NASA Ocean Biology and Biogeochemistry contracts NNX06AH32G, NNX08AB10G, and NNX06AH86G.

References

1. H. R. Gordon, O. B. Brown, and M. M. Jacobs, "Computed relationships between the inherent and apparent optical properties," Appl. Opt. **14**, 417–427 (1975).
2. H. R. Gordon, "Dependence of the diffuse reflectance of natural waters on the Sun angle," Limnol. Oceanog. **34**, 1484–1489 (1989).
3. A. Morel and B. Gentili, "Diffuse reflectance of oceanic waters. II. Bidirectional aspects," Appl. Opt. **32**, 6864–6879 (1993).
4. A. Morel, K. Voss, and B. Gentilli, "Bidirectional reflectance of oceanic waters: a comparison of modeled and measured upward radiance fields," J. Geophys. Res. **100**, 13143–13150 (1995).
5. J. R. V. Zaneveld, "A theoretical derivation of the dependence of the remotely sensed reflectance of the ocean on the inherent optical properties," J. Geophys. Res. **100**, 13135–13142 (1995).
6. T. J. Petzold, "Volume scattering functions for selected ocean waters," Tech. Rep. (Scripps Institution of Oceanography, 1972), pp.72–78.
7. G. Kullenberg, "Scattering of light by Sargasso Sea water," Deep-Sea Res. **15**, 423–432 (1968).
8. N. G. Jerlov, "Optical measurements in the eastern North Atlantic," Medd. Oceanogr. Inst. Göteborg **30**, 1–40 (1961).
9. M. E. Lee and M. R. Lewis, "A new method for the measurement of the optical volume scattering function in the upper ocean," J. Atmos. Ocean. Technol. **20**, 563–571 (2003).
10. M. Chami, E. Marken, J. J. Stamnes, G. Khomenko, and G. Korotaev, "Variability of the relationship between the particulate backscattering coefficient and the volume scattering function measured at fixed angles," J. Geophys. Res. **111**, C05013 (2006).
11. J.-F. Berthon, E. Shybanov, M. E.-G. Lee, and G. Zibordi, "Measurements and modeling of the volume scattering function in the coastal northern Adriatic Sea," Appl. Opt. **46**, 5189–5203 (2007).
12. M. S. Twardowski, WET Labs, Inc., Department of Research, 70 Dean Knauss Drive, Narragansett, Rhode Island, 02882, USA, and C. Moore, J. M. Sullivan, M. Slivkoff, S. Freeman, and J. R. V. Zaneveld are preparing a manuscript to be called "Volume scattering functions for selected ocean waters: revisited."
13. T. Oishi, "Significant relationship between the backward scattering coefficient of sea water and the scatterance at 120°," Appl. Opt. **29**, 4658–4665 (1990).
14. R. A. Maffione and D. R. Dana, "Instruments and methods for measuring the backward scattering coefficient of ocean waters," Appl. Opt. **36**, 6057–6067 (1997).

15. E. Boss and W. S. Pegau, "Relationship of light scattering at an angle in the backward direction to the backscattering coefficient," Appl. Opt. **40**, 5503–5507 (2001).
16. J. C. Kitchen and J. R. V. Zaneveld, "A three-layered sphere model of the optical properties of phytoplankton," Limnol. Oceanogr. **37**, 1680–1690 (1992).
17. R. M. Pope and E. S. Fry, "Absorption spectrum (380–700 nm) of pure water. II. Integrating cavity measurements," Appl. Opt. **36**, 8710–8723 (1997).
18. M. S. Twardowski, J. M. Sullivan, P. L. Donaghay, and J. R. V. Zaneveld, "Microscale quantification of the absorption by dissolved and particulate material in coastal waters with an ac-9," J. Atmos. Ocean. Technol. **16**, 691–707 (1999).
19. J. M. Sullivan, M. S. Twardowski, J. R. Zaneveld, C. Moore, A. Barnard, P. L. Donaghay, and B. Rhoades, "The hyperspectral temperature and salinity dependent absorption of pure water, salt water and heavy salt water (D_2O) in the visible and near-IR wavelengths (400–750 nm)," Appl. Opt. **45**, 5294–5309 (2006).
20. J. R. V. Zaneveld, J. C. Kitchen, and C. C. Moore, "The scattering error correction of reflecting-tube absorption meters," Proc. SPIE **2258**, 44–55 (1994).
21. M. S. Twardowski, H. Claustre, S. A. Freeman, D. Stramski, and Y. Huot, "Optical backscattering properties of the "clearest" natural waters," Biogeosciences **4**, 1041–1058 (2007).
22. X. Ma, J. Q. Lu, R. S. Brock, K. M. Jacobs, P. Yang, and X. Hu, "Determination of complex refractive index of polystyrene microspheres from 370 to 1610 nm," Phys. Med. Biol. **48**, 4165–4172 (2003).
23. Y. C. Agrawal, A. Whitmire, O. A. Mikkelsen, and H. C. Pottsmith, "Light scattering by random shaped particles and consequences on measuring suspended sediments by laser diffraction," J. Geophys. Res. **113**, C04023 (2008).
24. X. Zhang, L. Hu, and M.-X. He, "Scattering by pure seawater: effect of salinity," Opt. Express **17**, 5698–5710 (2009).
25. G. R. Fournier and J. L. Forand, "Analytic phase function for ocean water," Proc. SPIE **2258**, 194–201 (1994).
26. J. L. Forand and G. R. Fournier, "Particle distribution and index of refraction estimation for Canadian waters," Proc. SPIE **3761**, 34–44 (1999).
27. E. Boss, M. S. Twardowski, and S. Herring, "Shape of the particulate beam spectrum and its inversion to obtain the shape of the particle size distribution," Appl. Opt. **40**, 4885–4893 (2001).
28. M. S. Twardowski, E. Boss, J. B. Macdonald, W. S. Pegau, A. H. Barnard, and J. R. V. Zaneveld, "A model for estimating bulk refractive index from the optical backscattering ratio and the implications for understanding particle composition in case I and case II waters," J. Geophys. Res. **106**, 14129–14142 (2001).
29. J. M. Sullivan, M. S. Twardowski, P. L. Donaghay, and S. Freeman, "Using optical scattering to discriminate particle types in coastal waters," Appl. Opt. **44**, 1667–1680 (2005).
30. M. Jonasz and G. R. Fournier, *Light Scattering by Particles in Water: Theoretical and Experimental Foundations* (Academic, 2007).
31. E. Boss, W. S. Pegau, M. Lee, M. S. Twardowski, E. Shybanov, G. Korotaev, and F. Baratange, "The particulate backscattering ratio at LEO-15 and its use to study particle composition and distribution," J. Geophys. Res. **109**, C01014 (2004).
32. A. L. Whitmire, E. Boss, T. J. Cowles, and W. S. Pegau, "Spectral variability of the particulate backscattering ratio," Opt. Express **15**, 7019–7031 (2007).